Available online at www.sciencedirect.com
SCIENCE DIRECT®
International Journal of Mass Spectrometry 233 (2004) 207–214
International Journal of Mass Spectrometry
www.elsevier.com/locate/ijms

Electron impact ionization studies with aeronomic molecules

B.K. Antony [a,b,*], K.N. Joshipura [a], N.J. Mason [b]

[a] *Department of Physics, Sardar Patel University, Vallabh Vidyanagar-388 120, Gujarat, India*
[b] *Department of Physics and Astronomy, Open University, Milton Keynes MK7 6AA, UK*

Received 13 October 2003; accepted 21 December 2003

Abstract

Total ionization cross-sections for electrons in the energy range from threshold to 2000 eV are calculated for the molecules O_2, N_2O, NO_2, ClO, OClO, Cl_2O, SF_5CF_3, NO_3 and N_2O_5. The total inelastic cross-sections determined in the spherical complex potential formalism are used to calculate the total ionization cross-sections. The present total ionization cross-sections are found to be consistent with experimental measurements, where they exist.

Keywords: Aeronomic molecules; Total ionization cross-section; Spherical complex potential

1. Introduction

In the Earth's upper atmosphere solar ultraviolet (UV) radiation is absorbed by its constituent molecules leading to ionization liberating free electrons. This "ionized" region of the atmosphere is therefore a weak plasma and is known as the *ionosphere*. At altitudes above 60 km the density of these free electrons is sufficient to affect the propagation of electromagnetic waves. Longer wavelength radio signals can be reflected off the ionosphere allowing radio communications to be propagated "over the horizon". Shorter wavelength radio signals pass through the ionosphere but are nonetheless affected by it. These shorter wavelengths are used by satellites for imaging the earth, and the ionosphere affects the received images in a manner similar to way the atmospheric absorption of visible wavelengths leads to the observed "twinkling" of the stars.

Atmospheric ionization is also produced by high energy particles emitted from the Sun and the cosmic background—so-called "cosmic rays". Although the amount of ionization produced by such particles is generally much less than that produced by solar radiation at night (when there is very little or no solar illumination), however, at times of high solar activity they may be important and, due to their high energy, are able to penetrate deeper into the atmosphere than solar UV. Indeed it has been speculated that such particles may play a role in nucleation of water droplets that lead to cloud formation, hence providing a link between cloud formation (and hence global climate cycles) and the solar sunspot cycle [1,2] while more recently a link between ozone depletion and cosmic radiation has also been suggested [2].

Therefore, it is important to be able to determine the electron impact ionization cross-sections for electron interactions with aeronomic species. The ionization cross-sections of the common atmospheric species, such as oxygen, nitrogen and water, are of course, well established but the ionization cross-sections of trace species are often unknown. In this paper, we report the results of a simple formalism to estimate electron ionization cross-sections from several aeronomic species for which there currently exists little or no experimental data, including several key radical species, for which experiments are impractical. These should not be regarded as definitive but provide an estimate that should encourage the development of more rigorous theoretical calculations and, where practical, experimental measurement.

2. Methodology

A spherical complex potential formalism has been used to generate the total inelastic cross-section for these molecules. A semi-empirical approach [3,4] called the "Complex Scattering Potential-Ionization Contribution" (CSP-*ic*) method

* Corresponding author.
E-mail address: bk_antony@rediffmail.com (B.K. Antony).

1387-3806/$ – see front matter © 2004 Elsevier B.V. All rights reserved.
doi:10.1016/j.ijms.2003.12.037

is then used to derive the total ionization cross-section Q_{ion} from the calculated Q_{inel}. The total inelastic cross-section Q_{inel} may be written as,

$$Q_{inel}(E_i) = Q_{ion}(E_i) + \Sigma Q_{exc}(E_i) \quad (1)$$

where the first term is the total cross-section for all allowed ionization processes and the second term is the sum over total excitation cross-sections for all accessible electronic transitions. The second term arises mainly from the low-lying dipole allowed transitions for which the cross-section decreases rapidly at higher energies. This becomes less important than the first term at energies well above the ionization threshold [5,6]. Hence, we have,

$$Q_{inel}(E_i) \geq Q_{ion}(E_i) \quad (2)$$

The complex scattering potential is generated from the spherically averaged charge densities of the target molecules, as described in our CSP-*ic* approach [3,4]. The single-center target charge density is obtained by a linear combination of constituent atomic charge densities, renormalized to account for covalent bonding and the total number of electrons present in the molecule [3]. In the case of N_2O_5 and SF_5CF_3, two centers were assumed. For N_2O_5 we have chosen one at $–NO_2$ and other at $–NO_3$ as the N–O bond distance (1.53 Å) is larger than N=O bond distance (1.2 Å) [7]. In SF_5CF_3 the S–C bond length (1.96 Å) [8] is the largest and so we considered one center at S and other at C. These centers are then added together and renormalized as above. Using this molecular charge density, we construct the real part of the complex potential [4] $V_{opt} = V_R + iV_I$, which is the sum of static (V_{st}), exchange (V_{ex}) and polarization (V_p) potentials,

$$V_R = V_{st}(r) + V_{ex}(r, E_i) + V_p(r, E_i) \quad (3)$$

The imaginary part (V_I), accounts for the total loss of scattered flux into all the allowed channels of electronic excitation and ionization. We have used a model potential, given by Staszewska et al. [9], which is quasi-free, Pauli-blocking, dynamic absorption potential (V_{abs}) given in au, as

$$V_{abs}(r, E_i) - \frac{1}{2}\rho(r)v_{loc}\sigma_{ee} = -\rho(r)\left(\frac{T_{loc}}{2}\right)^{1/2}\left(\frac{8\pi}{10k_F^3E_i}\right)\theta(p^2 - k_F^2 - 2\Delta) \times (A_1 + A_2 + A_3) \quad (4)$$

Here, v_{loc} is the local speed of the incident electron, and σ_{ee} denotes the average total cross-section of the binary collision of the incident electron with a target electron. The local kinetic energy of the incident electron is obtained from,

$$T_{loc} = E_i - V_R = E_i - (V_{st} + V_{ex} + V_p) \quad (5)$$

In Eq. (4), $p^2 = 2E_i$, k_F is the Fermi wave vector and Δ is an energy parameter. $\theta(x)$ is the Heaviside step-function, such that $\theta(x) = 1$ for $x > 0$, and is zero otherwise. The dynamic functions A_1, A_2 and A_3 which are given in Staszewska et al. [9] depend differently on $\rho(r)$, I, Δ and E_i. The parameter Δ assumed to be fixed in the original model determines a threshold below which $V_{abs} = 0$, and the ionization or excitation is prevented energetically. Here, we have modified Δ such that at impact energies close to the (vertical) ionization threshold I, the excitations to the discrete states also take place, but as E_i increases valence ionization becomes dominant, together with the possibility of ionization of the inner electronic shells. In the range of intermediate energies the V_{abs} shows a rather excessive loss of flux into the inelastic channels. The potential also penetrates in the region of inner electronic shells, which are of course harder to be excited or ionized. In order to rectify this behavior of this potential, we choose $\Delta \approx I$ for low E_i and $\Delta > I$ at E_i near the position of the peak of Q_{inel}. Thus, our modification [3,4] expresses Δ as a slowly varying function of E_i around I.

After the formulation of the complex optical potential, we solve the Schrödinger equation with the modified V_{abs}, using the appropriate boundary conditions. The real and imaginary part of the phase shifts $\delta_l = \mathrm{Re}\delta_l + i\,\mathrm{Im}\delta_l$ are generated for various partial waves l. Thus, we get the S-matrix elements,

$$S_l = \exp(2i\delta_l) \quad (6)$$

which can be rewritten as,

$$S_l = \exp(2i\delta_l) = \eta_l \exp(2i\mathrm{Re}\delta_l) \quad (7)$$

where the quantity $\eta_l = \exp(-2\mathrm{Im}\delta_l)$ is called the "inelasticity" or "absorption" factor [10]. The term absorption being understood in the sense that particle disappears from incident channel. Thus, we obtain the total inelastic cross-section is given by [10],

$$Q_{inel} = \frac{\pi}{k^2}\sum_{l=0}^{\infty}(2l+1)(1-\eta_l^2) \quad (8)$$

As the cross-section of interest in many applications is Q_{ion}, we must extract this from Q_{inel}. There is no rigorous way to get the former from the latter. Hence, in order to determine Q_{ion} from our calculated Q_{inel}, we define the following quantity for $E_i \geq I$.

$$R(E_i) = \frac{Q_{ion}(E_i)}{Q_{inel}(E_i)}, \quad \text{such that } 0 \leq R \lesssim 1 \quad (9)$$

We require that $R = 0$ when $E_i \leq I$. For a number of stable molecules, like H_2O, CH_4, SiH_4, etc., for which the experimental cross-sections Q_{ion} are known accurately [11,12], the ratio R rises steadily as the energy increases above the threshold, and it is found that

$$R(E_i)\begin{cases} = R_p, & \text{at } E_i = E_p \\ \cong 1, & \text{for } E_i \gg E_p \end{cases} \quad (10)$$

where E_p stands for the incident energy at which the calculated Q_{inel} attains its maximum. R_p stands for the value of R at $E_i = E_p$, and as per our discussion in [3,4] we choose $R_p \cong 0.7$. This behavior is attributed to the faster fall of the second term ΣQ_{exc} in Eq. (1).This choice follows from

the general observation that at energies close to the peak of the ionization cross-section the contribution of the molecular Q_{ion} is about 70–80% of the total inelastic cross-sections Q_{inel}. The higher limit of 80% is observed only in the targets having very high ionization potentials, like Ne (IP = 21.56 eV) [3]. The molecules discussed in this paper, however, have the ionization potential ranging from 10.35 to 12.89 eV, so we have selected the lower limit of 70%. Such an approximation may introduce an uncertainty of some 5% in general as R_p might actually vary from ∼0.7 to 0.74.

For calculating the Q_{ion} from Q_{inel} we need R as a continuous function of energy $E_i \geq I$, hence we represent [3,4] the ratio R in the following manner.

$$R(E_i) = 1 - f(U);$$
$$R(E_i) = 1 - C_1\left[\frac{C_2}{U+a} + \frac{\ln(U)}{U}\right] \quad (11)$$

Here, U is the dimensionless variable defined through, $U = E_i/I$.

The functional form of $f(U)$ in Eq. (11) is adopted from the fact that, as E_i increases above I, the ratio R increases and approaches unity, since the ionization contribution rises and the discrete excitation term in Eq. (1) decreases. The discrete excitation cross-sections, dominated by dipole transitions, fall off as $\ln(U)/U$ at high energies. Accordingly, the decrease of the function $f(U)$ must also be proportional to $\ln(U)/U$ in the high range of energy. However, the two term representation of $f(U)$ given in Eq. (11) is more appropriate since the first term in the square bracket ensures a better energy dependence at low and intermediate E_i. The Eq. (11) involves dimensionless parameters C_1, C_2 and a, that reflect the target properties. To determine these parameters, we note the following three conditions on the ratio R. (i) It is zero at and below the ionization threshold. (ii) It behaves in accordance with Eq. (10) at the peak position E_p, and (iii) it approaches 1 asymptotically for E_i sufficiently larger than E_p. These parameters are tabulated in Tables 1 and 2 for the present molecules. The Eqs. (9)–(11) define the present CSP-*ic* approach [3,4].

For more complex targets it is also possible to adopt additivity rules that sum ionization cross-sections for constituent atoms/molecular groups of the larger molecule. Since several of the targets we investigated have no experimental or theoretical data we have also used a modified additivity rule (MAR) to explore whether it is possible to evaluate ionization cross-sections for complex targets from measurements/calculations of small molecular components. This method, if shown to be reliable, might allow us to "guestimate" ionization cross-sections for biological molecules [3]. Our MAR method may be described as follows. The individual atomic inelastic cross-sections are calculated after adjusting the ionization potentials of the constituent atoms to allow for the ionization potential of the molecule. These cross-sections are then added together to get the MAR-Q_{inel}. Then, by using the ratio as described above in Eq. (11), we estimate the MAR-Q_{ion}. The geometry (bond length, etc.) will also play an important role in the evaluation cross-section, as the charge density is extended in case of a molecule (see below).

Table 1
Ionization potential and molecular geometries of some of molecules studied[a]

Target	IP (eV)	Bond distance (Å)	Angle (°)
O [25]	13.62		
Cl [25]	12.97		
O_2 [25]	12.07	1.207	
NO_2 [25]	11.23	1.193	ONO = 134.1
N_2O [25]	12.89	N≡N = 1.124; N=O = 1.184	ONO = 134.1
ClO [26]	11.20	1.576	
OClO [27]	10.35	1.470	OClO = 117.4
Cl_2O	10.91	1.696	ClOCl = 110.9

[a] See Ref. [7,8,24] for SF_5CF_3, N_2O_5 and NO_3, respectively.

Table 2
Parameters used in Eq. (11) for the molecules studied

Target	Parameters		
	a	C_1	C_2
O_2	8.495	−0.931	−10.202
N_2O	12.649	−1.371	−9.959
NO_2	17.380	−1.630	−11.277
ClO	9.222	−1.092	−9.360
OClO	6.330	−0.674	−10.873
Cl_2O	7.463	−0.588	−14.389
SF_5CF_3	17.632	−1.638	−11.372
NO_3	12.898	−1.380	−10.074
N_2O_5	13.041	−1.372	−10.234

3. Results and discussions

This theoretical approach (CSP-*ic*) was used to estimate values of Q_{ion} for various atmospheric gases. To test the validity (and accuracy) of our approximations we calculated Q_{ion} for several targets for which there exists a reasonable experimental data set and compare our results with two other approximate formalisms, Binary-Encounter-Bethe (BEB) [13] and Deutch–Märk (DM) methods [14,15]. The BEB model [13] combines the Mott cross-section with the high incident energy behavior of the Bethe cross-section [16]. The theory uses a simple analytic formula for the ionization cross-section per atomic/molecular orbital. The total ionization cross-section for a target is obtained by summing these orbital cross-sections. A different approach called the DM formalism [14,15] makes use of the static target properties, like electronic sub-shell radii, binding energies and a dynamic, i.e., energy-dependent function to obtain the shell-wise contribution to Q_{ion}.

In Fig. 1, our present CSP-*ic* results for O_2 are compared with BEB theory [13], DM formalism [15] and experiments of Krishnakumar and Srivastava [17] and Rapp and Englander-Golden [18]. The present results and BEB

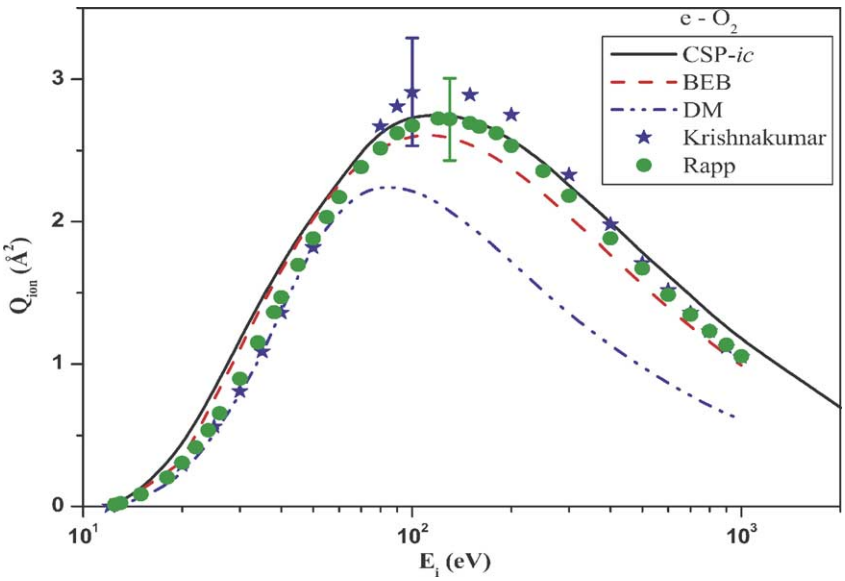

Fig. 1. Total ionization cross-sections for e–O_2 scattering. (—) Complex Scattering Potential-Ionization Contribution, CSP-*ic* (present method). (– – –) Binary-Encounter-Bethe (BEB) [13]. (– · · –) Deutch-Märk, DM [15]. (★) Krishnakumar and Srivastava [17]. (●) Rapp and Englander-Golden [18].

theory are slightly above the experiments near the threshold region; however, the present results seem to be in good agreement with the experiments at all other energies, including the peak. In contrast, the BEB theory seems to underestimate the experiments above 70 eV and the results of the DM formalism lies below all the experimental results and the present calculations.

In Fig. 2, we present the total ionization cross-sections of N_2O along with BEB theory [13] and experiments of Rapp and Englander-Golden [18] and Iga et al. [19]. We have also plotted the total (single) ionization cross-sections measurements of Lopez et al. [20]. Both theories lie within the experimental uncertainty in the experiments. The BEB method seems to overestimate the cross-section below the peak of the ionization cross-section. We have not plotted here the modified additive theoretical values of Deutsch et al. [21] but these are slightly higher than the present values as well as experiment.

The results for NO_2 are presented in the Fig. 3 along with the experiments of Lindsay et al. [22] and Lukic et al. [23]. The total (single) ionization cross-sections measurements of Lopez et al. [20] seem to underestimate the values of the peak cross-section. This underestimation may be ascribed to the fact that only the single ionization is measured by Lopez et al. and therefore would be expected to be lower that a calculated total ionization cross-section. Nevertheless,

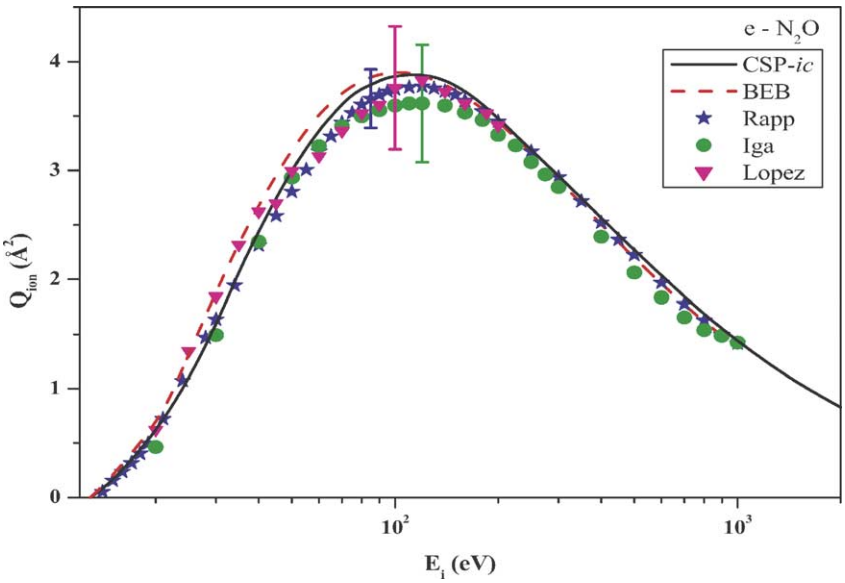

Fig. 2. Total ionization cross-sections for e–N_2O scattering. (—) CSP-*ic*. (– – –) BEB [13]. (★) Rapp and Englander-Golden [18]. (●) Iga et al. [19]. (▼) Lopez et al. [20].

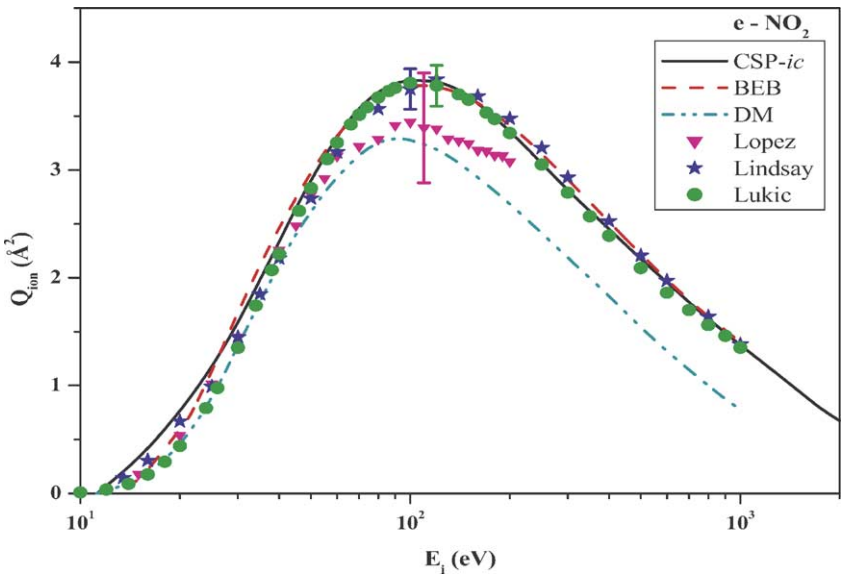

Fig. 3. Total ionization cross-sections for e–NO_2 scattering. (—) CSP-*ic*. (– – –) BEB [13]. (– · · –) DM [15]. (▼) Lopez et al. [20]. (★) Lindsay et al. [22]. (●) Lukic et al. [23].

the present results are still within the experimental uncertainties of the measurements. The BEB theory [13] and DM formalism [15] are also compared with present results. Both experiments are in good agreement with present results and also with the BEB theory while DM formalism seems to underestimate the cross-section above 50 eV. In contrast, the modified additive results for NO_2 by Deutsch et al. [21] (not shown here) overestimates the cross-section.

Figs. 1–3 suggest that the present methodology (CSP-*ic*) is capable of providing reasonable estimates of Q_{ion} for simple molecules. Therefore, we have used this method to estimate cross-sections for several other aeronomic species for which there is currently little or no data. The first molecules we have studied are the three chlorine oxides, ClO, OClO and Cl_2O, which play a key role in stratospheric ozone depletion, the ClO radical as an ozone scavenger and OClO and Cl_2O by acting as sinks for chlorine release by photolysis of CFC compounds. Fig. 4 shows Q_{ion} for the ClO radical. No previous data exist for this target.

The MAR-Q_{ion} would seem to overestimate the cross-sections for ClO below the peak after which it falls faster than the present results of ClO. This is because in the MAR we have considered only the ionization potential of the molecule. However, the geometry (bond length, etc.) may also play an important role in the evaluation of cross-section, as the charge density is extended in case of a molecule.

In Fig. 5, the total ionization cross-sections for both OClO and Cl_2O are plotted. The cross-section for Cl_2O is higher

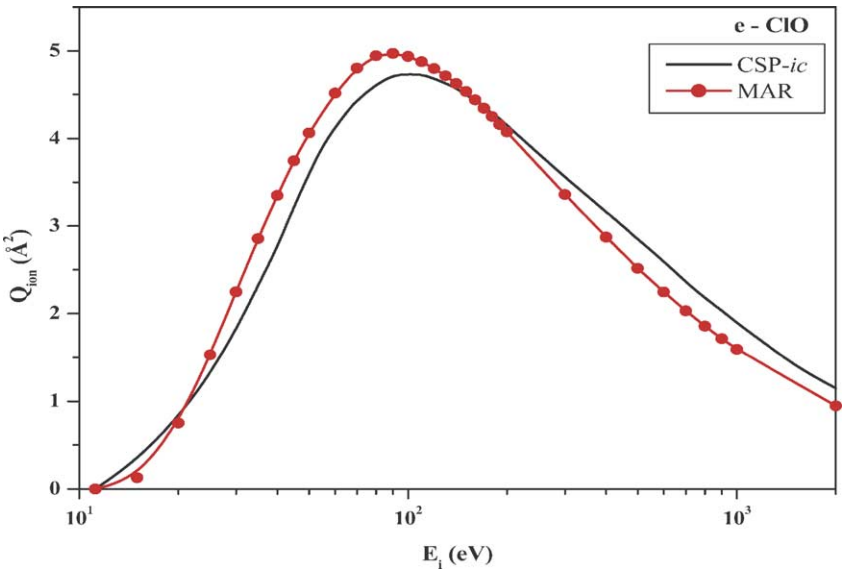

Fig. 4. Total ionization cross-sections for e–ClO scattering. (—) CSP-*ic*. (–●–) Modified additivity rule (MAR).

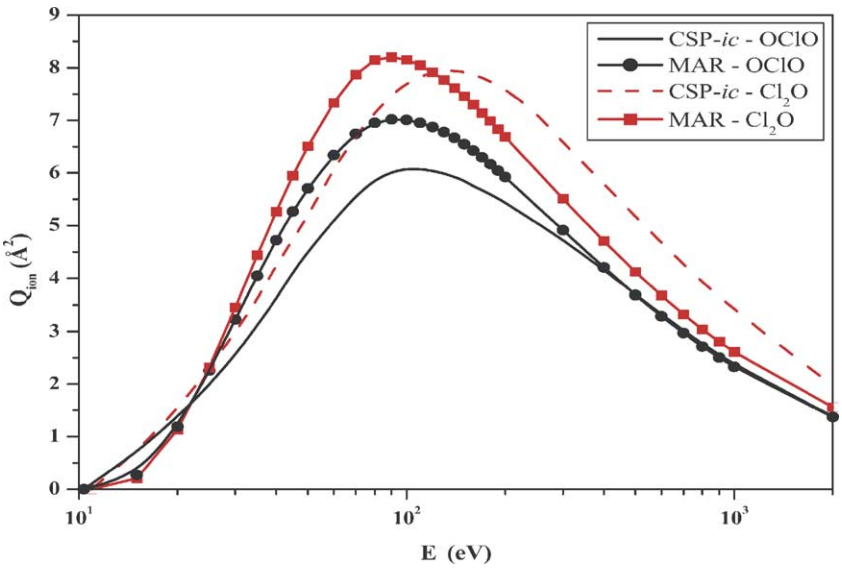

Fig. 5. Total ionization cross-sections for e–OClO and Cl_2O scattering. (—) CSP-*ic*-OClO. (–●–) MAR-OClO. (– – –) CSP-*ic*-Cl_2O. (–■–) MAR-Cl_2O.

than that of OClO because the Cl–O bond distance is larger for Cl_2O and it also has 42 electrons compared to 33 electrons for OClO. No previous experimental or theoretical results are known for these molecules. We also present the curve for the MAR cross-sections for OClO and Cl_2O. Both MAR results overestimate the respective cross-section in the lower and intermediate energies. At higher energies MAR is in good agreement with the present results for OClO, while it is lower in the case of Cl_2O. This may be due the small bond length in case of OClO compared to the Cl_2O.

In Fig. 6, we present Q_{ion} for SF_5CF_3. SF_5CF_3 is the strongest greenhouse gas yet found (being almost 20,000 more active than carbon dioxide) in the atmosphere and is currently the subject of extensive experimental investigations but at present there is no measurement of its ionization cross-section. Since the structural properties of SF_5CF_3 are not yet clear, we have used the modified additive rule to estimate Q_{ion}. Once again this addition is likely to lead to an overestimate in the actual cross-section.

In Fig. 7, we present the total ionization cross-section for NO_3 radical. As no previous results are available, we have also plotted the MAR cross-section of NO_3. This summed cross-section seems to overestimate Q_{ion} at lower energies, while giving similar results at higher energies. This is due to the similar ionization potentials of these species and because of the D_{3h} structure [24] of NO_3 molecule ensures that the O atoms are spatially spread out allowing the additivity to be a better estimate at higher energies.

In our last Fig. 8, we have plotted Q_{ion} for N_2O_5. N_2O_5 is a key sink compound in the stratosphere for nitric oxides

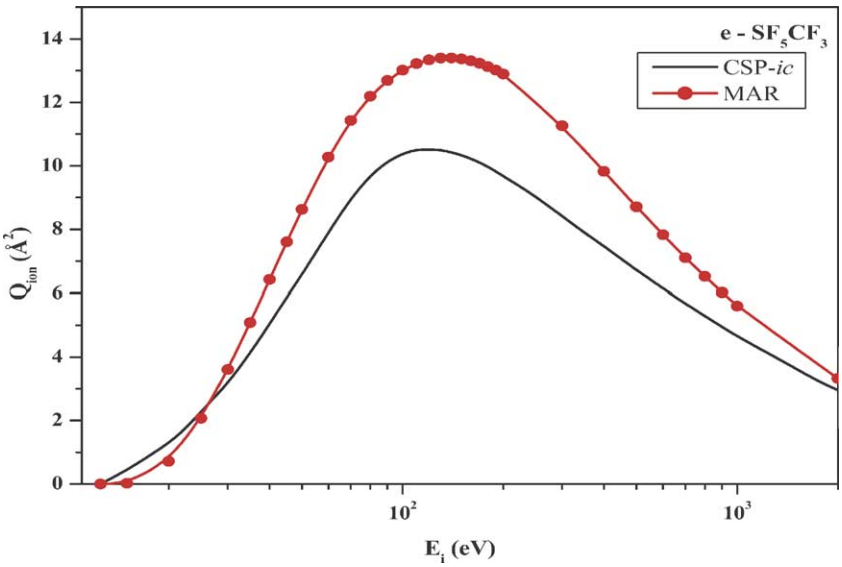

Fig. 6. Same as Fig. 4, but for e–SF_5CF_3 scattering.

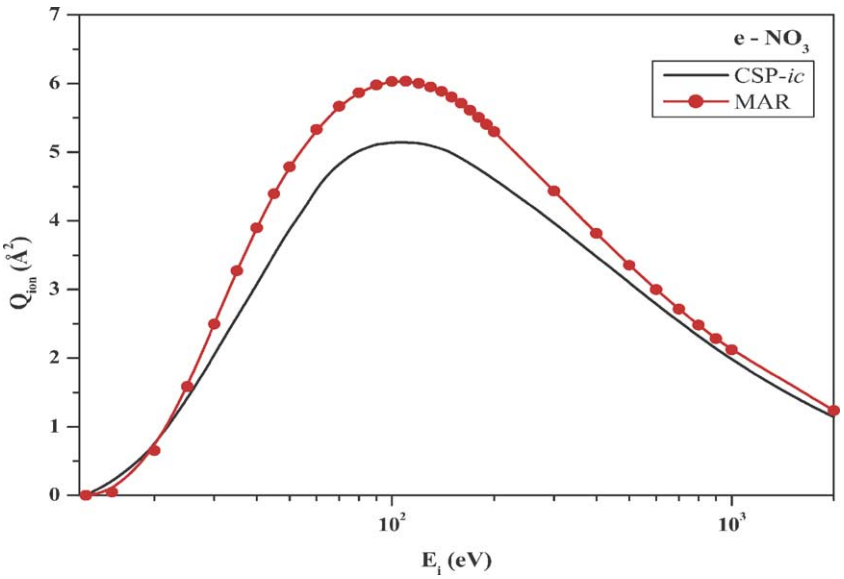

Fig. 7. Same as Fig. 4, but for e–NO_3 scattering.

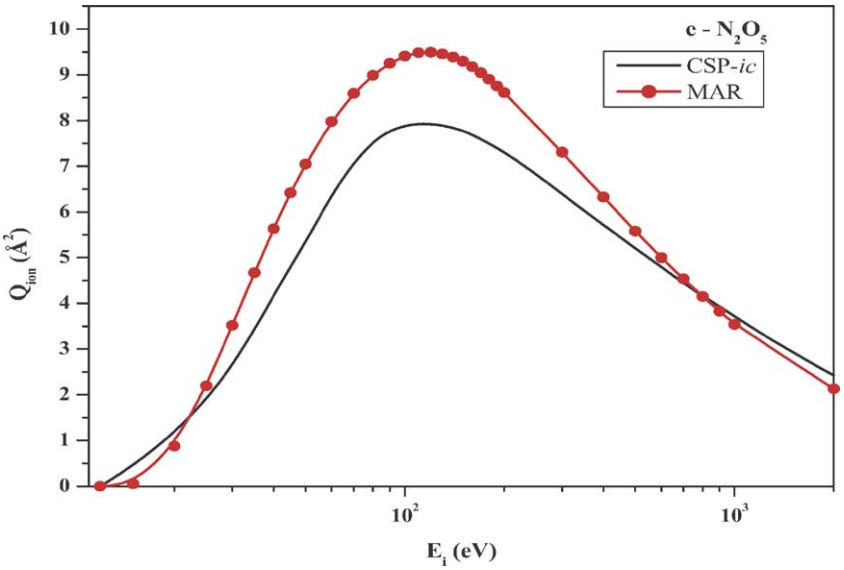

Fig. 8. Same as Fig. 4, but for e–N_2O_5 scattering.

which are capable of initiating ozone loss. As there are no previous results are available for N_2O_5, we have also plotted the MAR cross-section of N_2O_5. As expected from discussions above this additivity overestimates the calculated N_2O_5 cross-section.

4. Conclusions

A simple theoretical method called CSP-*ic* is used to evaluate total ionization cross-sections for several atmospheric gases. The results obtained for O_2, NO_2 and N_2O are in good agreement with BEB theory and other experiments. We have then presented the first estimates of the ionization cross-sections for the radicals ClO and NO_3, the stratospheric compounds OClO, Cl_2O and N_2O_5 and the greenhouse gas SF_5CF_3 for which there are currently no theoretical or experimental results available. Using a MAR, we have also shown that ionization cross-sections for larger more complex polyatomics may be estimated albeit with the likelihood of overestimating the magnitude of the cross-section. It is to be hoped that these calculations will initiate further theoretical calculations and, where practical, experimental effort.

Acknowledgements

B.K.A. thanks the Commonwealth (UK) for a scholarship award. K.N.J. thanks the Department of Science and Tech-

nology, New Delhi, India, for a research grant under which a part of this work has been done.

References

[1] H. Svensmark, E. Friis-Christensen, J. Atmos. Solar-Terrestrial Phys. 59 (1997) 1225.
[2] M. Michaud, M. Lepage, L. Sanche, Phys. Rev. Lett. 81 (1998) 2807.
[3] K.N. Joshipura, B.K. Antony, V. Minaxi, J. Phys. B: At. Mol. Opt. Phys. 35 (2002) 4211;
K.N. Joshipura, B.K. Antony, Phys. Letts. A 289 (2001) 323.
[4] K.N. Joshipura, M. Vinodkumar, B.K. Antony, N.J. Mason, Eur. Phys. J. D 23 (2003) 81, and references therein.
[5] A. Zecca, G.P. Karwasz, R.S. Brusa, C. Szmytkowski, J. Phys. B 24 (1991) 2747.
[6] A. Zecca, G.P. Karwasz, R.S. Brusa, C. Szmytkowski, Phys. Rev. A 45 (1992) 2777.
[7] A.F. Voegele, C.S. Tautermann, T. Loerting, K.R. Liedl, Phys. Chem. Chem. Phys. 5 (2003) 487.
[8] P. Limao-Vieira, P.A. Kendall, S. Eden, N.J. Mason, J. Heinesch, M.J. Hubin-Franskin, J. Delwiche, A. Giuliani, Radiat. Phys. Chem. 68 (2003) 193, and references therein.
[9] D. Staszewska, D.W. Schwenke, D. Thirumalai, D.G. Truhlar, Phys. Rev. A 29 (1984) 3078.
[10] C.J. Joachain, Quantum Collision Theory, North Holland Press, Amsterdam, 1983.
[11] G.P. Karwasz, R.S. Brusa, A. Zecca, La Rivista Del Nuovo Cimento 24 (2001) 1.
[12] R. Basner, M. Schmidt, V. Tarnovsky, K. Becker, H. Deustch, Int. J. Mass Spectrom. Ion Processes 171 (1997) 83.
[13] Y.-K. Kim, W. Hwang, N.M. Weinberger, M.A. Ali, M.E. Rudd, J. Chem. Phys. 106 (1997) 1026;
Y.-K. Kim, M.E. Rudd, Phys. Rev. A 50 (1994) 3954, see also NIST Web-Site, http://physics.nist.gov/PhysRefData/Ionization/EII_table.html.
[14] H. Deutsch, K. Becker, S. Matt, T.D. Märk, Int. J. Mass Spectrom. 197 (2000) 37, and references therein.
[15] M. Probst, H. Deutsch, K. Becker, T.D. Märk, Int. J. Mass Spectrom. 206 (2001) 13.
[16] M. Inokuti, Rev. Mod. Phys. 11 (1971) 297.
[17] E. Krishnakumar, S.K. Srivastava, Int. J. Mass Spectrom. Ion Processes 113 (1992) 1.
[18] D. Rapp, P. Englander-Golden, J. Chem. Phys. 43 (1965) 1464.
[19] I. Iga, M.V.V.S. Rao, S.K. Srivastava, J. Geophys. Res. 101 (1996) 9261.
[20] J. Lopez, V. Tarnovsky, M. Gutkin, K. Becker, Int. J. Mass Spectrom. 225 (2003) 25.
[21] H. Deutsch, K. Becker, T.D. Märk, Int. J. Mass Spectrom. 167 (1997) 503.
[22] B.G. Lindsay, M.A. Mangan, H.C. Straub, R.F. Stebbings, J. Chem. Phys. 112 (2000) 9404.
[23] D. Lukic, G. Josifov, M.V. Kurepa, Int. J. Mass Spectrom. 205 (2001) 1.
[24] R.P. Wayne, The Nitrate Radical: Physics, Chemistry, and the Atmosphere, Commission of the European Communities, Belgium, 1990.
[25] R. Lide, CRC Handbook of Chemistry and Physics, CRC Press LLC, Boca Raton, FL, 2003.
[26] S.J. Kim, Y.J. Kim, C.H. Shin, B.J. Mhin, T.D. Crawford, J. Chem. Phys. 117 (2002) 9703.
[27] http://Webbook.Nist.gov.